Correlation between Molecular Packing and Optical Properties in Different Crystalline Polymorphs and Amorphous Thin Films of *mer*-Tris(8-hydroxyquinoline)aluminum(III)

Martin Brinkmann,*[,†,‡] Gregory Gadret,[†,§] Michele Muccini,[†] Carlo Taliani,[†] Norberto Masciocchi,*[,∥,⊥,▽] and Angelo Sironi[∥]

Contribution from the Istituto di Spettroscopia Molecolare, Consiglio Nazionale delle Ricerche, via P. Gobetti 101, 40129 Bologna, Italy, Dipartimento di Chimica Strutturale e Stereochimica Inorganica e Centro CNR CSSMTBO, Università di Milano, via Venezian 21, 20133 Milano, Italy, and Dipartimento di Scienze Chimiche, Fisiche e Matematiche, Università dell'Insubria, via Lucini 3, 22100 Como, Italy

Received October 7, 1999

Abstract: Since 1987, high-luminance low-voltage driven devices based on tris(8-hydroxyquinoline)aluminum(III) (Alq_3) opened the route to design low-cost large area displays and illuminators. Despite the large number of studies devoted to this material, very little is known about its basic structural and optical properties in the solid state. Therefore, we have investigated the structure(s) and the correlation between *inter*molecular interactions and optical properties in various Alq_3 systems, including solution, amorphous thin films, and different crystalline forms. Two novel unsolvated polymorphs of Alq_3, namely, α-Alq_3 and β-Alq_3, have been synthesized and their crystalline structures determined from X-ray diffraction data on powders (α) and single crystals (β). Crystals of α-Alq_3 are triclinic, space group *P*-1, $a = 6.2586(8)$ Å, $b = 12.914(2)$ Å; $c = 14.743(2)$ Å, $\alpha = 109.66(1)°$; $\beta = 89.66(1)°$, and $\gamma = 97.68(1)°$; crystals of β-Alq_3 are triclinic, space group *P*-1, $a = 8.4433(6)$ Å, $b = 10.2522(8)$ Å; $c = 13.1711(10)$ Å, $\alpha = 108.578(1)°$, $\beta = 97.064(1)°$, and $\gamma = 89.743(1)°$. Both these crystal structures consist of a racemic mixture of the *mer* isomer, but are characterized by different molecular packings involving well-defined short contacts between quinoxaline ligands belonging to symmetry-related Alq_3 molecules with interligand spacings in the 3.5−3.9 Å range. A third "high-temperature" phase, γ-Alq_3, was found to contain orientationally disordered *mer*-Alq_3 molecules, lying about a *32* position of the trigonal *P*-31*c* space group, with $a = 14.41(1)$ Å and $c = 6.22(1)$ Å. In addition, a hemichlorobenzene adduct of Alq_3 was also prepared and structurally characterized (monoclinic, space group $P2_1/n$, $a = 10.786(1)$ Å, $b = 13.808(2)$ Å, $c = 16.928(2)$ Å, $\beta = 97.90(2)°$). Investigations of the different crystal phases, as well as of amorphous thin films and solutions by absorption, fluorescence excitation, fluorescence, and Raman spectroscopy, allowed the effect of the molecular packing on the emission properties to be elucidated, the nature of the photoexcitations to be clarified, and the vibrational fingerprints of the α and β crystalline forms to be highlighted. The spectral position of fluorescence is found to be correlated with both the molecular density of the packing and the length of interligand contacts between neigboring Alq_3 molecules as a consequence of different dispersive and dipolar interactions as well as different $\pi-\pi$ orbital overlaps (the shorter the contacts, i.e., the denser the crystal, the more the fluorescence is red-shifted). The low-temperature (4.2 K) vibronic structure of the fluorescence spectrum of Alq_3 is resolved for the first time. It is assigned to the Franck−Condon activity of an in-plane bending mode at ca. 525 cm^{-1}, and it is symptomatic of the ligand-centered nature of the optical transitions. From the analysis of the vibronic progression the existence of a strong electron−phonon coupling involving the 525 cm^{-1} mode with a Huang−Rhys factor of ca. 2.6 ± 0.4 is inferred. The origin of the amorphous nature of the vacuum-sublimed thin films is here explained on the basis of the accessibility of many different $\pi-\pi$ links between homo- and heterochiral Alq_3 molecules.

Introduction

Since the pioneering work of Tang and van Slyke who first demonstrated the possibility to design high-luminance low-voltage driven devices based on Alq_3, a large amount of work has been dedicated to the development of organic electroluminescent diodes (OLEDs).[1] Alq_3 is a stable metal chelate that can be sublimed to yield amorphous thin films and stands as one of the most successful organic materials used in OLEDs. The typical OLED structure reported initially by Tang et al. consists of two layers, a hole transport layer involving a diamine-like molecule and an electron-transport layer based on Alq_3, which are sandwiched between two charge-injecting electrodes.[2] Multilayered devices in which the emission wavelength can be

† Consiglio Nazionale delle Ricerche.
‡ Present address: Massachusetts Institute of Technology, Department of Material Science and Engineering, Cambridge, MA 02139.
§ Present address: Max Planck Institut für Polymer Forschung, Mainz, Germany.
∥ Università di Milano.
⊥ Università dell'Insubria.
▽ Fax: +39-02-70635288. E-mail: norbert@csmtbo.mi.cnr.it.

(1) Tang, C. W.; Van Slyke, S. A. *Appl. Phys. Lett.* **1987**, *51*, 913.
(2) Friend, R. H.; Gymer, R. W.; Holmes, A. B.; Burroughes, J. H.; Marks, R. N.; Taliani, C.; Dos Santos, D. A.; Brédas, J.-L.; Lögdlund, M.; Salaneck, W. R. *Nature* (*London*) **1999**, *397*, 121. Hamada, Y. *IEEE Trans. Electron Devices* **1997**, *44*, 1206.

10.1021/ja993608k CCC: $19.00
Published on Web 05/13/2000

tuned by means of the applied voltage have been reported, opening some interesting perspectives for the design of low-cost large-area LED displays.[3] Most of the recent studies have been devoted to the optimization of the device characteristics,[4] to the improvement of the morphological stability,[5] to the understanding of the charge-transport mechanisms,[6] and to the tuning of the OLED emission spectrum.[7,8] However, there are only a few systematic investigations of the correlations existing between the molecular packing, the morphological properties in thin films, and the corresponding optical/electronic properties in conjugated molecular materials.[9] In particular, changes in the molecular packing are expected to influence the characteristics of the excited electronic states as evidenced in the case of aromatic hydrocarbons[10] and secondary dicarboxamides where various arene−arene geometries can be obtained and lead to a large variety of fluorescence behaviors.[11−15]

Concerning the optical properties of Alq_3, few studies have been dedicated to the fluorescence in solution and sublimed thin films,[6,16,17] focusing mainly on the high quantum yield of fluorescence, a value of ca. 0.30 being recently reported for vacuum-deposited films.[18] However, it must be stressed that the optical properties of thin films are those of an amorphous-like material consisting, as postulated recently by several authors,[19,20] of a mixture of the two geometrical isomers of Alq_3, called meridianal (*mer*) and facial (*fac*), i.e., disordered media without any controlled and well-defined molecular organization which give rise to inhomogeneously broadened spectra. It appears therefore as a major requirement to synthesize controlled and well-defined Alq_3-based molecular architectures to investigate the effect of molecular packing on the optical properties. Surprisingly, in the case of Alq_3, only two isostructural solvated structures, namely, Alq_3(MeOH) and Alq_3(ethyl acetate)$_{1/2}$, have been determined so far,[21,22] and no crystal structure of the unsolvated forms of Alq_3 has ever been reported. Also still unclear is the possibility of thermal interconversion between the *mer* and *fac* isomers of Alq_3 when sublimed in high vacuum. Such an isomeric transformation was first inferred from NMR measurements in deuterated chloroform when the temperature was increased to ca. 115 °C.[23]

From the theoretical point of view ab initio calculations of the ground-state properties of the isolated Alq_3 molecules have been performed[20] quite recently for the two *mer* and *fac* isomers. It was found that the HOMO of the *mer* isomer, which is present in the crystalline state (see Schmidbaur et al.[21]), is split in three nearly degenerate molecular orbitals. The two *mer* and *fac* isomers are characterized by permanent dipoles of ca. 4 and 7 D, respectively. More recent computational calculations based on density functional theory (DFT) have investigated the effect of charge addition and metal−Alq_3 interactions on the electronic structure and molecular geometry of Alq_3.[20,24] Nevertheless, no assignment of the lowest allowed optical transition and no theoretical investigations of the electronic excited states have so far been reported.

This paper contains crystallographic results which are mostly based on the newly emerging technique of ab initio X-ray powder diffraction (XRPD) methods, recently promoted by us in the field of coordination chemistry using conventional, but well conditioned, laboratory equipment.[25] The structures reported in the following sections, inter alia, represent some of the most complex species characterized by this method and, accordingly, show that, even when it is unable to provide atomic resolution, XRPD can afford very valuable information in the field of molecular compounds, such as crystal packing and the nature of the intermolecular contacts. We have been able to isolate three novel unsolvated polymorphs of Alq_3 and to determine their crystal structures, which show the presence of close contacts between adjacent 8-hydroxyquinoline ligands belonging to symmetry-related Alq_3 molecules. Given the different polymorphs of Alq_3, the correlations existing between the observed molecular architectures and the corresponding optical properties, probed by absorption, fluorescence emission, and excitation as well as Raman spectroscopies, are highlighted. The effects of intermolecular interactions have been investigated for Alq_3 systems ranging from solutions of increasing concentration to amorphous thin films and ultimately to ordered crystalline systems, including a hemichlorobenzene-solvated form of Alq_3. The optical properties and the amorphous nature of the thin films are accordingly analyzed on the basis of the intrinsic polymorphism of Alq_3.

Experimental Section

(a) Synthesis of the Different Alq_3 Polymorphs. α-Alq_3 is quantitatively obtained by the entrainer sublimation technique by loading Alq_3 powder (Aldrich, 99.9% purity) in a ceramic boat placed in a quartz tube (diameter ca. 5 cm and length ca. 80 cm), which is heated at the sublimation temperature of Alq_3. Under a constant flux of nitrogen (99.99%), crystalline needles of Alq_3 are formed on the

(3) Shen, Z.; Burrows, P. E.; Bulovic, V.; Forrest, S. R.; Thompson, M. E. *Science* **1997**, *276*, 2009.
(4) McElvain, J.; Antoniadis, H.; Hueschen, M. R.; Miller, J. N.; Roitman, D. M.; Sheats J. R.; Moon, R. L. *J. Appl. Phys.* **1996**, *80*, 6002.
(5) (a) Do, L. M.; Han, E. M.; Yamamoto, N.; Fujihira M. *Thin Solid Films* **1996**, *273*, 202. (b) Do, L. M.; Han, E. M.; Yamamoto, N.; Fujihira M.; Kanno, T.; Yoshida, S.; Maeda, A.; Ikushima, A. J. *J. Appl. Phys.* **1994**, *76*, 5118.
(6) (a) Burrows, P. E.; Shen, Z.; Bulovic, V.; McCarty, D. M.; Forrest, S. R.; Cronin, J. A.; Thompson, M. E. *J. Appl. Phys.* **1996**, *79*, 7991. (b) Blom, P. W. M.; de Jong, M. J. M.; van Munster, M. G. *Phys. Rev. B* **1997**, *55*, 656. (c) Muckl, A. G.; Berleb, S.; Brutting, W.; Schwoerer, M. *Synth. Met.*, in press.
(7) (a) Tang, C. W.; Van Slyke, S. A.; Chen, C. H. *J. Appl. Phys.* **1989**, *65*, 3610. (b) Adachi, C.; Tsutsui, T.; Saito, S. *Appl. Phys. Lett.* **1989**, *55*, 1489.
(8) Hopkins, T. A.; Meerholz, K.; Shaheen, S.; Anderson, M. L.; Schmidt, A.; Kippelen, B.; Padias, A. B.; Hall, H. K., Jr.; Peyghambarian, N.; Armstrong, N. R. *Chem. Mater.* **1996**, *8*, 344.
(9) Taliani, C.; Biscarini, F.; Muccini, M. In *Semiconducting Polymers, Chemistry, Physics and Engineering*; Van Hutten, P. F., Hadziioannou, G., Eds.; Wiley-VCH: Weinheim, 1999.
(10) (a) Stevens, B. *Nature* (*London*) **1961**, *192*, 725. (b) Stevens, B. *Spectrochim. Acta* **1962**, *18*, 439.
(11) (a) Lewis, F. D.; Yang, J. S.; Stern, C. L. *J. Am. Chem. Soc.* **1996**, *118*, 2772. (b) Lewis, F. D.; Yang, J. S. *J. Phys. Chem. B* **1997**, *101*, 1775.
(12) Pope, M. In *Electronic processes in organic crystals*; Oxford University Press: Oxford, 1982; p 26.
(13) De Vries Reilingh, D. N.; Rettschnick, R. P. H. *J. Chem. Phys.* **1971**, *54*, 2722.
(14) Kobayashi, T. *J Aggregates*; World Scientific Publishing Co.: Singapore, 1996; p 95.
(15) Kirstein, S.; Möhwald, H. *Adv. Mater.* **1995**, *7*, 460.
(16) Ohnesorge, W. E.; Rogers, L. B. *Spectrochim. Acta* **1959**, *15*, 27.
(17) Lytle, F. E.; Storey, D. R.; Jurich, M. E. *Spectrochim. Acta* **1973**, *29*, 1357.
(18) Garbuzov, D. Z.; Bulovic, V.; Burrows P. E.; Forrest, S. R. *Chem. Phys. Lett.* **1996**, *249*, 433.
(19) Chen, C. H.; Shi, J. *Coord. Chem. Rev.* **1998**, *171*, 161.
(20) (a) Curioni, A.; Boreo, M.; Andreoni, W. *Chem. Phys. Lett.* **1998**, *294*, 263. (b) Curioni, A.; Andreoni, W.; Treusch, R.; Himpsel, F. J.; Haskal, E.; Seidler, P.; Kakar, S.; von Buuren, T.; Terminello, L. J. *Appl. Phys. Lett.* **1998**, *72*, 1575.
(21) Schmidbaur, H.; Lettenbauer, J.; Wilkinson, D. L.; Müller, G.; Kumberger, O. *Z. Naturforsch.* **1991**, *B46*, 901.
(22) Fujii, I.; Hirayama, N.; Ohtani, J.; Kodama, K. *Anal. Sci.* **1996**, *12*, 153.
(23) Baker, B. C.; Sawyer, D. T. *Anal. Chem.* **1968**, *40*, 1945.
(24) (a) Johansson, N.; Osada, T.; Staström, S.; Salaneck, W. R.; Parente, V.; Dos Santos, D. A.; Crispin, X.; Brédas, J.-L. *J. Phys. Chem.* **1999**, *111*, 2157. (b) Curioni, A.; Andreoni, W. *J. Am. Chem. Soc.* **1999**, *121*, 8592.
(25) Masciocchi, N.; Sironi, A. *J. Chem. Soc., Dalton Trans.* **1997**, 4643.

colder part of the quartz tube. Alternatively, α-Alq_3 is obtained by recrystallization from spectroscopic grade acetone or by heating, above 180 °C, the solvated phase $Alq_3(C_6H_5Cl)_{1/2}$ obtained from C_6H_5Cl solutions. Single-crystal growth by recrystallization was performed in the dark under an inert environment (N_2) to avoid degradation of Alq_3 by oxidative condensation of the ligand which occurs in the presence of O_2 and H_2O.[26−28]

The largest needles of α-Alq_3 obtained by sublimation have typical dimensions of ca. 20 × 20 × 400 μm^3. Under diffraction conditions, these needles proved to be polycrystalline in agreement with their morphology showing parallel bundles of thin threads. Among the multitude of α-Alq_3 needles obtained by recrystallization from acetone, a few larger and flat crystals could be found, and attributed to a distinct polymorph, herafter β. The *pseudo*hexagonally shaped β-Alq_3 single crystals of typical size 50 × 500 × 500 μm^3 proved to be suitable for conventional diffraction methods. The nonsolvated character of the α and β polymorphs was originally ascertained by IR and Raman analyses which did not reveal any trace of acetone.

Powders of the γ-Alq_3 phase have been prepared by heating α-Alq_3 or $Alq_3(C_6H_5Cl)_{1/2}$ under a nitrogen atmosphere above the (irreversible) α → γ phase transition temperature located at ca. 395 °C. Annealing temperatures higher than 410 °C are found to result in sublimation to α-Alq_3 (ΔH = ca. 49 kJ mol^{-1}).[29] The presence of contaminants (brown material), probably due to polycondensation of the ligands, prevented the isolation of pure γ-Alq_3, which has therefore not been submitted to further optical characterization.

Thin films of Alq_3 were obtained by vacuum sublimation at a base pressure of ca. 10^{-7} mbar. Substrates consist of either quartz slides or passivated Si(100). Passivation of the Si(100) substrates was performed by dipping into 10% HF solution for 1 min and rinsing with deionized water. The starting Alq_3 material (Aldrich, 98%) was purified by the usual entrainer sublimation technique as described above. The deposition rate was kept at a constant value of ca. 1 nm/min, and the substrate temperature, T_s was regulated in the range 300−450 K. As described elsewhere,[30] the films of Alq_3 deposited onto passivated Si(100) consist of a loose or tight network of noncoalescing amorphous droplets, depending on the deposited thickness.

Differential scanning calorimetry (DSC) and thermogravimetric analysis (TGA) were performed with the aid of a Perkin-Elmer DSC7/TGA7 modular instrument.

(b) Crystallography. X-ray Powder Diffraction Analysis of $Alq_3(C_6H_5Cl)_{1/2}$. X-ray powder diffraction data were obtained with graphite-monochromated Cu Kα radiation (λ = 1.5418 Å) on a Philips PW1820 vertical-scan powder diffractometer, equipped with parallel (Soller) slits. HV setting: 40 kV and 40 mA. Slits used: DS (1.0°), AS (1.0°), RS (0.2 mm). Gently ground Alq_3 powder was cautiously deposited in the hollow (ca. 0.5 mm deep) of a glass specimen holder by the top-loading technique. Data were collected at room temperature in the 5−95° range, in the $\theta-2\theta$ mode, step scan with $\Delta 2\theta$ = 0.02° and a fixed time of 10 s/step. The lowest 2θ (21) peaks (located by standard peak search methods) were fed in the trial and error indexing routines of TREOR.[31] Reasonable agreement within the monoclinic system leads to the following unit cell parameters a = 10.81 Å, b = 13.79 Å, c = 16.91 Å, β = 97.9°; $F(21)^{32}$ = 23(0.016, 57). No rational transformations of this unit cell into high symmetries could be found. Systematic absences indicated $P2_1/n$ as the probable space group.

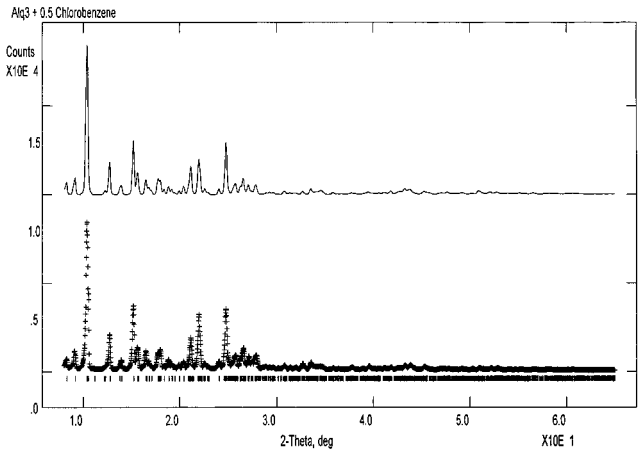

Figure 1. Rietveld refinement plot of the $Alq_3(C_6H_5Cl)_{1/2}$ phase. Measured (bottom) and calculated (top) profiles and peak markers are shown.

Although visual comparison of the X-ray powder pattern with those computed from the already published coordinates for the methanol and ethyl acetate solvates[21,22] did not grant structure similarity with the known phases, the derived lattice parameters and the determined space group strongly suggested that Alq_3 molecules are arranged in a similar manner. Therefore, as the initial model, a complete Alq_3 was included in an "ideal" position and refined by the Rietveld method as a rigid body (adding external observations to the normal least-squares procedure in the form of restraints). Subsequent difference Fourier clearly revealed a C_6H_5Cl moiety (disordered about an inversion center), which was then also included in the final refinement, performed using GSAS,[33] which allows bond parameters to be restrained to known values. One isotropic thermal parameter was refined (0.05(3) $Å^2$). The contribution of the H atoms to the scattering factors was neglected. The background was refined using a six-term cosine series. The angular dependence of the peak widths (of pseudo-Voigt shape) was modeled using the Caglioti et al. formula,[34] with the V and Z parameters set to zero. Final Rp, Rwp, and R_F values were 0.17, 0.13, and 0.094, respectively. Figure 1 shows the final Rietveld refinement plot. A summary of crystal data and refinement parameters can be found in Table 1.

X-ray Powder Diffraction Analysis of Alq_3 (α-Phase). The yellow needle-shaped crystals afforded very weak diffraction spots. Repeated long (10 min/frame) exposures on a Siemens SMART three-circle diffractometer equipped with a CCD area detector allowed as many as 150 well-defined [with $I > 100\sigma(I)$] reflections per crystal to be detected, which, however, did not lead to any unambiguously determined unit cell, indicating the probable polycrystalline nature of the needles. Therefore, we resorted again to XRPD measurements, performed (on thoroughly ground Alq_3 needles and on sublimed powders) very much as described above for the C_6H_5Cl solvated phase. Preliminary XRPD data on what we have found to be the α-Alq_3 phase have been recently reported,[26b] but their modest quality, together with the limited observed range, could not afford any useful structural information. Interestingly, the powder diffraction pattern in our hands was of very good quality, but rather complex, as indicated by the presence of three intense, well resolved peaks within the $6° < 2\theta < 8°$ range, completely missed in the original report.[26b] On using the 15 well-resolved peak positions, TREOR[31] indicated, among others, a probable triclinic cell consistent with Z = 2 [a = 6.27 Å, b = 12.92 Å, c = 14.73 Å, α = 109.6°, β = 89.7°, γ = 97.7°; $F(16)$ = 57 (0.011, 24)]. No rational transformations of this unit cell into high symmetry could be found. The space group P-1 was initially assumed, and later confirmed by successful solution and refinement. Patterson maps and direct methods (EXPO[35]) based on the LeBail fit in the $5° < 2\theta < 65°$ range did not afford any reliable solution; however, using the real-

(26) (a) Papadimitrakopoulos, F.; Zhang, X.-M.; Thomsen D. L.; Higginson, K. A. *Chem. Mater.* **1996**, *8*, 1363. (b) Higginson, K. A.; Zhang, X.-M.; Papadimitrakopoulos, F. *Chem. Mater.* **1998**, *10*, 1017.

(27) Schmidt, A.; Anderson, M. L.; Aromstrong, R. N. *J. Appl. Phys.* **1995**, *78*, 5619.

(28) Sano, K.; Kawata, Y.; Urano, T.I.; Mori, Y. *J. Mater. Chem.* **1992**, *2*, 767.

(29) In contrast with our observations, these two endotherms were interpreted as "*denaturation*" of the "*normal*" *fac*- and *mer*-isomers of Alq_3, leading to "*a new type of* Alq_3" (from ref 28).

(30) Brinkmann, M.; Biscarini, F.; Ghedini, M.; Aiello, I.; Taliani, C. *Phys. Rev. B., Rapid Commun.*, in press.

(31) Werner, P. E.; Eriksson, L.; Westdahl, M. *J. Appl. Crystallogr.* **1985**, *18*, 367.

(32) De Wolff, P. M. *J. Appl. Crystallogr.* **1968**, *1*, 108. Smith, G. S.; Snyder, R. L. *J. Appl. Crystallogr.* **1979**, *12*, 60.

(33) Larson, A. C.; Von Dreele, R. B. LANSCE, MS-H805, Los Alamos National Laboratory, New Mexico, 1990.

(34) Caglioti, G.; Paoletti, A.; Ricci, F. P. *Nucl. Instrum. Methods* **1958**, *3*, 223.

Table 1. Summary of Crystal Data for $Alq_3(C_6H_5Cl)_{1/2}$ and Alq_3 (β-Phase), Including Data Collection and Refinement Details

empirical formula	$C_{30}H_{20.5}AlCl_{0.5}N_3O_3$	$C_{27}H_{18}AlN_3O_3$	$C_{27}H_{18}AlN_3O_3$
fw	515.72	409.43	409.43
cryst syst	monoclinic	triclinic	triclinic
space group	$P2_1/n$ (no. 14)	P-1 (no. 2)	P-1 (No.2)
a, Å	10.786(1)	6.2586(8)	8.4433(6)
b, Å	13.808(2)	12.914(2)	10.2522(8)
c, Å	16.928(2)	14.743(2)	13.1711(10)
α, deg	90	109.66(1)	108.578(1)
β, deg	97.90(2)	89.66(1)	97.064(1)
γ, deg	90	97.68(1)	89.743(1)
V, Å^3	2497.3(5)	1111.1(2)	1071.7(2)
Z	4	2	2
F(000)	1150	476	476
D(calcd), g cm^{-3}	1.372	1.373	1.424
μ, mm^{-1}	0.15	0.11	0.13
temp, K	293(2)	293(2)	293(2)
technique	powder diffraction	powder diffraction	single-crystal diffraction
diffractometer	Philips PW1820	Philips PW1820	Siemens SMART/CCD
λ, Å	1.5418	1.5418	0.71073
2θ range, deg	8−65	5−65	4−58
agreement indices	$R_F = 0.09$	$R_F = 0.10$	R1 = 0.059, wR2 = 0.103
profile agreement indices	Rp = 0.14, Rwp = 0.18	Rp = 0.11, Rwp = 0.14	na

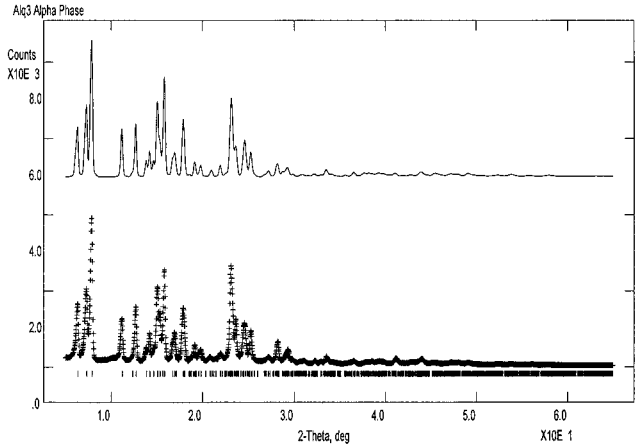

Figure 2. Rietveld refinement plot of the Alq_3 α-phase. Measured (bottom) and calculated (top) profiles and peak markers are shown.

space scavenger technique recently developed in this laboratory (PRISCON[36]), a 34-atom Alq_3 fragment could be approximately located and oriented in the unit cell. Further optimization was performed, after including H atoms in ideal positions, by lattice-constrained molecular mechanics,[37] which afforded a very good starting point for final (restrained) Rietveld refinement (Figure 2), performed using GSAS[33] ($U_{iso} = 0.07(5)$ Å^2). Instrumental parameters (background, peak shape, and their angular dependence) were treated as described above. Final Rp, Rwp, and R_F values were 0.11, 0.14, and 0.10, respectively.

On heating $Alq_3(C_6H_5Cl)_{1/2}$ in a vacuum at ca. 200 °C for 15 min, solvent evolution drives the complete transformation of the monoclinic crystals into the triclinic Alq_3 α-phase, which, however, shows a slightly modified XRPD pattern; the latter could be fully indexed and completely described by a slightly inflated α-phase, with lattice parameters of 6.299(1), 12.997(2), and 14.822(3) Å, and 109.57(1)°, 89.45(2)°, and 97.99(2)°, leading to a unit cell volume of about 1131 Å^3, i.e., 1.8% larger than that of the sublimed powders.

X-ray Single-Crystal Analysis of Alq_3 (β-Phase). Single-crystal X-ray diffraction data were collected at room temperature on a Siemens SMART three-circle diffractometer equipped with a CCD area detector, using graphite-monochromated Mo Kα radiation (λ = 0.710 73 Å). HV setting: 45 kV and 40 mA. Initial unit cell parameters and an orientation matrix were obtained from least-squares refinement on 44 reflections measured in three different sets of 15 frames each in the range $2° < 2\theta < 23°$. Approximately a full sphere of data within the limits $1° < 2\theta < 58°$ was collected by the ω scan technique with the frame width set to 0.3° and the sample−detector distance fixed at 4.96 cm with a beam exposure of 30 s/frame. The collected frames were then processed by the software SAINT for integration; an absorption correction was applied (SADABS; $T_{min} = 0.850$) on the 10 186 collected reflections ($R_\sigma = \Sigma[\sigma(F_o^2)]/\Sigma F_o^2 = 0.079$), 4790 of which are unique, with $R_{int} = \Sigma[F_o^2 - F_{mean}^2]]/\Sigma F_o^2 = 0.038$. The structure was solved by direct methods (SIR97[38]) and difference Fourier methods and subsequently refined by full-matrix least squares against F_o^2 using all the reflections and the program SHELXL97.[39] All non-hydrogen atoms were given anisotropic displacement parameters, while H atoms were included in calculated positions and refined riding on their parent carbon atoms with isotropic displacement parameters 1.2 times that of the pertinent carbon atom. Table 1 contains details of the crystal data and data collection and refinement procedures. Full lists of fractional atomic coordinates and bond distances and angles have been deposited as Supporting Information.

X-ray Powder Diffraction Analysis of Alq_3 (γ-Phase). Powders of a mixture of rapidly quenched γ-Alq_3 and of dark-brown polycondensed ligands (vide supra) were measured at room temperature as for the α-phase. All intense peaks could be successfully indexed by a trigonal unit cell (see Table 2). Density and symmetry considerations, geometric modeling, and simulation of the XRPD pattern and lattice-constrained molecular mechanics (in P-1)[37] clearly indicate the presence of Alq_3 molecules lying about the *32* symmetry position (at 0, 0, 1/4) of the centrosymmetric P-31c space group. Thus, this phase contains orientationally disordered *mer*-Alq_3 molecules, possibly derived from a high-temperature rotor phase present above 395 °C, where dynamic equalization of the quinoxaline ligands, without any bond breaking, can occur. However, the low(er) quality of the observed XRPD pattern, due to the presence of contaminant materials, did not allow a quantitative Rietveld fit.

(c) Spectroscopy. Fluorescence measurements in the temperature range 4.2−300 K have been performed in a helium bath cryostat. Fluorescence was excited by the 365.5 nm line of an UV extended argon ion laser and detected by an optical multichannel analyzer coupled to a CCD array. For the fluorescence excitation (FLE) measurements the excitation source was a 300 W xenon lamp coupled to a monochromator interfaced to a PC. The monochromators used for the

(35) Altomare, A.; Burla, M. C.; Cascarano, G.; Giacovazzo, C.; Guagliardi, A.; Moliterni, A. G. G.; Polidori, G. *J. Appl. Crystallogr.* **1995**, *28*, 842.

(36) Masciocchi, N.; Bianchi, R.; Cairati, P.; Pilati, T.; Sironi, A. *J. Appl. Crystallogr.* **1994**, *27*, 426.

(37) Mercandelli, P. L.; Moret, M.; Sironi, A. *Inorg. Chem.* **1998**, *37*, 2563.

(38) Altomare, A.; Burla, M. C.; Camalli, M.; Cascarano, G. L.; Giacovazzo, C.; Guagliardi, A.; Moliterni, A. G. G.; Polidori, G.; Spagna, R. *J. Appl. Crystallogr.* **1999**, *32*, 115.

(39) Sheldrick, G. M. SHELXL-97: Program for structure refinement, University of Göttingen, Germany, 1997.

Table 2. Synoptic Collection of Crystal Data for Various Crystal Phases Containing Mq_3 Fragments

phase	solvent (clathrated)	system	space group	*a*, Å	*b*, Å	*c*, Å	α, deg	*β*, deg	*γ*, deg	*V*, Å^3	*Z*	ref or CCDC code
Alq_3 (α)	none	triclinic	*P*-1	6.26	12.91	14.74	109.7	89.7	97.7	1111	2	this work
Alq_3 (*β*)	none	triclinic	*P*-1	8.44	10.25	13.17	108.6	97.1	89.7	1072	2	this work
Alq_3 (*γ*)	none	trigonal	*P*-31*c*	14.41	14.41	6.22	90	90	120	1118	2	this work
Alq_3	CH_3OH	monoclinic	$P2_1/n$	10.78	13.21	16.79		97.8		2370	4	HQUALA01
Alq_3[a]	0.5 $CH_3OCOC_2H_5$	monoclinic	$P2_1/n$	10.97	13.32	16.85		98.6		2434	4	22
Alq_3	0.5 CH_3COCH_3	monoclinic	$P2_1/n$	10.94	13.19	16.87		98.4		2407	4	JIWLAC
Alq_3	0.5 C_6H_5Cl	monoclinic	$P2_1/n$	10.79	13.81	16.93		97.9		2497	4	this work
Gaq_3[b]	none	"amorphous"										54
Gaq_3	CH_3OH	monoclinic	$P2_1/n$	10.84	13.27	16.79		98.0		2392	4	VIYZUY
Gaq_3	C_2H_5OH	monoclinic	$P2_1/n$	11.23	13.32	16.72		94.2		2496	4	YINRIW
Gaq_3[c]	0.5 $C_2H_5OC_2H_5$	monoclinic	$P2_1/n$	11.02	13.28	16.92		98.0		2452	4	54
Inq_3	C_2H_5OH	monoclinic	$P2_1/n$	11.31	13.55	16.82		94.9		2568	4	YINRES01
Tlq_3	H_2O	monoclinic	*C*2/*c*	23.90	15.48	13.84		118.5		4500	8	YINROC
Sbq_3	none	orthorhombic	$P2_12_12_1$	8.16	9.40	28.66				2199	4	YINRUI
Crq_3	CH_3OH	monoclinic	$P2_1/n$	10.96	13.21	16.90		97.4		2427	4	QUICRM
Mnq_3	CH_3OH	monoclinic	$P2_1/n$	10.85	13.20	17.28		97.6		2453	4	MNQOLM10
Mnq_3	C_2H_5OH	monoclinic	$P2_1/n$	11.10	13.22	17.08		95.3		2497	4	ZEMZEW
Mnq_3	0.5 *n*-$C_6H_{13}OH$	monoclinic	$P2_1/n$	11.20	13.34	17.20		97.1		2550	4	MNQOLH10
Feq_3	C_2H_5OH	monoclinic	$P2_1/n$	11.19	13.42	16.73		94.3		2504	4	RESDOI
Coq_3	C_2H_5OH	monoclinic	$P2_1/n$	11.39	12.77	16.67		92.6		2424	4	YINRAO
Ruq_3	$CHCl_3$	monoclinic	$P2_1/n$	10.92	13.20	16.92		98.4		2412	4	ZULTAB
Rhq_3	$CHCl_3$	monoclinic	$P2_1/n$	10.99	13.07	16.89		97.7		2405	4	ZULTEF
Osq_3	$CHCl_3$	monoclinic	$P2_1/n$	10.96	13.11	16.99		98.3		2416	4	ZULSUV

[a] Originally formulated as $Alq_3 \cdot 0.25(CH_3COCH_2)_2$. [b] It is very possible that the Gaq_3 (amorphous) needles and the Alq_3 (α-phase), for which PD data clearly show high crystallinity and *standard* single-crystal techniques fail to afford suitable Bragg reflections (see the text), belong to the same structural class. [c] This phase was erroneously presented as pure Gaq_3, in clear disagreement with its chemical preparation, observed lattice metrics, and space group analogies with the above-mentioned monoclinic phases.

selection of both the excitation and detection wavelengths are characterized by a spectral resolution of about 10 nm. The exciting source and the FLE signal from the sample were simultaneously detected by two photomultipliers with the lock-in technique to normalize the FLE spectra with respect to the excitation intensity. FLE low temperature measurements were performed with the samples placed in the sample holder of a helium coldfinger cryostat. For the crystalline phases, measurements have been performed both on smoothly powdered polycrystalline samples fixed on a quartz plate and on isolated single crystals. Single crystals were carefully mounted in a homemade sample holder, which could be fit alternatively into the bath or the coldfinger cryostat. The samples were initially flushed with He gas and slowly cooled to 4.2 K to avoid mechanical damage of the very brittle crystals. The near-infrared excited Raman scattering measurements were performed with a RFS 100 Bruker Raman interferometer in a backscattering configuration with a resolution of 2 cm^{-1}. A diode pumped cw Nd:YAG laser was used for excitation at $\lambda_{exc} = 1064$ nm, with a laser spot of ca. 0.3 mm diameter.

Results

Analysis of the crystal structures of Alq_3. Crystal Structure of $Alq_3(C_6H_5Cl)_{1/2}$. This species crystallizes in the monoclinic space group $P2_1/n$ and consists of a host lattice of Alq_3 molecules occluding chlorobenzene molecules disordered about an (statistical) inversion center. This supramolecular arrangement is far from being unusual, since all the solvated Mq_3 crystal phases (M = a trivalent metal; see Table 2) are strictly isomorphous, with the notable exception of the hydrated Tlq_3 phase, which displays C-centered monoclinic symmetry.[40] Notably, the closed cavity of the monoclinic Mq_3 species hosts either small (CH_3OH, C_2H_5OH, $CHCl_3$) or large(r) noncentrosymmetric (thus disordered) solvents in a 1:1 or 1:0.5 proportion, respectively.

In the crystal, Alq_3 molecules are linked by short (<3.6 Å) intermolecular $\pi-\pi$ contacts to symmetry-related (−1) fragments and to the clathrated chlorobenzene (S) molecules, leading to a periodic stack, along (100), of aromatic rings of the Q′/Q/S sequence. Accordingly, 3 × 3.6 Å neatly reproduces the *a* parameter of 10.79 Å. With reference to Figure 3, the quinoxaline rings involved in such interactions are those labeled with A. A schematic drawing of the crystal packing can be found in Figure 4a.

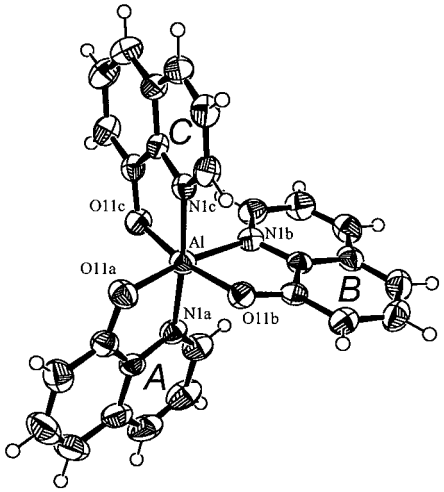

Figure 3. ORTEP drawing of the Alq_3 molecule (from the *β*-phase), with partial labeling scheme. Hydrogen atoms are omitted for clarity. Thermal ellipsoids are drawn at the 30% probability level. The ring labeling for the three hydroxyquinoline ligands in *mer*-Alq_3 described in the text is also schematically drawn. Selected geometrical parameters: Al−O11a 1.850(2) Å, Al−O11b 1.860(2) Å, Al−O11c 1.857(2) Å, Al−N1a 2.050(2) Å, Al−N1b 2.087(2) Å, Al−N1c 2.017(2) Å; (trans angles) O11a−Al−N1b 171.46(8)°, O11b−Al−O11c 168.22(8)°, N1a−Al−N1c 173.82(8)°; (cis chelate angles) O11a−Al−N1a 83.63(8)°, O11b−Al−N1b 81.36(7)°, O11c−Al−N1c 83.43(7)°; other cis angles in the 89.36(8)−97.52(7)° range.

The antiparallel juxtaposition of the Q/Q′ ligands along the (100) direction, favored by dipolar interactions, is depicted at the bottom of Figure 4. The slipped, graphitic-like arrangement is characterized by Q/Q′ close contacts of ca. 3.6 Å. No other

(40) Bankowski, Yu. A.; Bel'skii, V. K.; Pech, L. Ya.; Ashaks, Ya. V. *Russ. J. Inorg. Chem.* **1993**, *38*, 1862.

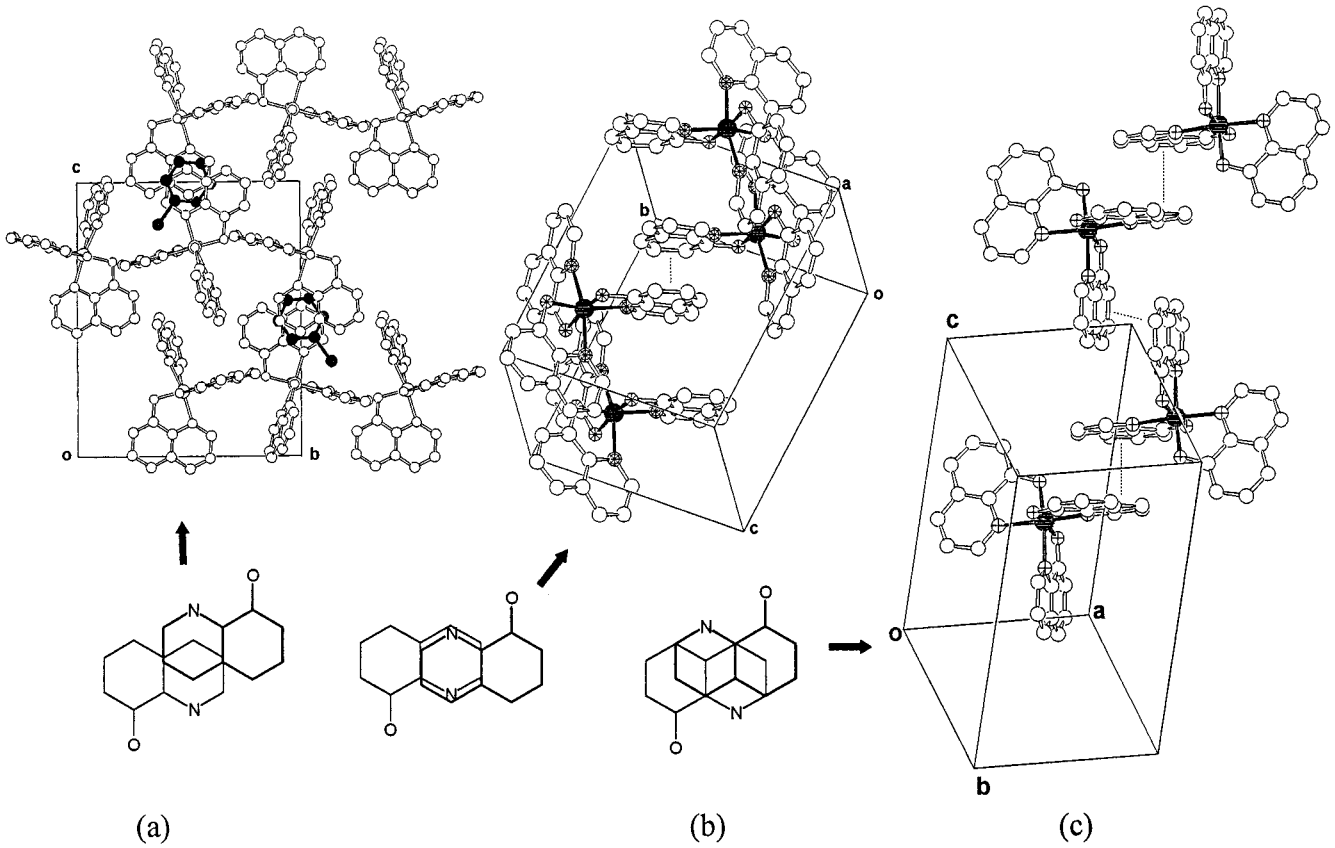

Figure 4. Crystal packing of (a) the $Alq_3(C_6H_5Cl)_{1/2}$ [down (1,0,0)], (b) the Alq_3 α-phase [down (3 −1 1)], and (c) the Alq_3 β-phase [down (121)] showing the short $\pi-\pi$ contacts between neighboring molecules (dashed lines) and in (a) the clathrated chlorobenzene molecules (in black). The relative shifts of the $\pi-\pi$ stacked aromatic rings are also drawn.

evident $\pi-\pi$ interactions involve the remaining quinoxaline ligands (Q/Q′ distance of ca. 7.5 Å). In agreement with this description, in all other isomorphous phases, given the presence of aliphatic guest molecules, only Q/Q′ dimers are present, in clear contrast with earlier reports of 1-D and even 2-D arrays.[21,22]

Crystal Structure of Alq_3 (α-Phase). The structure of this phase has a triclinic symmetry and does not bear any significant subgroup relation or rational transformation to any pseudomonoclinic crystal packing. Thus, α-Alq_3 is a definite outlier in the list of Table 2. Accordingly, a different packing mode is present, with much looser intermolecular interatomic distances of ca. 3.9 Å, linking the symmetry-related Q/Q′ rings of the B type (see Figure 3). This stacking [along (−1 0 1)] occurs in a rather different mode, as depicted in Figure 4, with pyridine rings of antiparallel Q fragments facing each other in an almost eclipsed manner. Such interactions only involve adjacent quinoxaline ligands Q/Q′ and therefore do not afford 1-D polyaromatic stacks throughout the crystal lattice. A schematic drawing of the crystal packing can be found in Figure 4b.

Crystal Structure of Alq_3 (β-Phase). The structure of the β-phase also has a typical triclinic unit cell and, as for α-Alq_3, cannot be related to the reported monoclinic crystal packing. Thus, β-Alq_3 also badly fits in the rather uniform list of Table 2. Since, among the studied phases, this is the only one which could be studied by conventional single-crystal methods, the complete Alq_3 geometry could be successfully unraveled (without the extensive modeling required for the powder diffraction analyses) and is briefly summarized in the caption of Figure 3, which contains an ORTEP drawing of an isolated Alq_3 molecule. A detailed comparison of the molecular geometries in this polymorph and in the methanolic solvate[21] clearly shows that the local distortions about the Al ion are very similar (Al−X bond distances and X−Al−Y angles match within 0.02 Å and 2.0°, respectively). Thus, the room temperature molecular conformation in the two crystals is not significantly affected by the crystal packing environment, and suggests, for *all* Alq_3 polymorphs, the presence of rather stiff molecular entities, thus enabling the above-mentioned (though, idealized) parametrization in the data analyses from XRPD data. The crystal packing in β-Alq_3 results in short distances of ca. 3.5 Å between neighboring symmetry-related quinoxaline ligands Q/Q′ stacked along the (−3 2 1, B/B′) and (0 −1 1, C/C′) directions. Such multiple nature of the $\pi-\pi$ links generates an extended one-dimensional chain, winding up along the (001) direction, of closely spaced Alq_3 molecules, which, therefore, show a higher density (see Table 1). A schematic drawing of the crystal packing can be found in Figure 4c.

Crystal Structure of Alq_3 (γ-Phase). The structure of the high-temperature γ-phase consists of a rather symmetric trigonal packing [a = 14.41(1) Å, c = 6.22(1) Å, $M(11) = 37$; $F(11) = 32$ (0.020, 17)] of *mer*-Alq_3 molecules lying about a *32* position of the centrosymmetric *P*-31*c* space group. Therefore, since these molecules lack any symmetry, they are necessarily disordered, with statistical 2-fold axes bisecting the *cis*-N−Al−O angles of the chelates. Interestingly, there is a simple relation between the lattice metrics of the α- and γ-phases (see Table 2): the high-temperature phase is reasonably obtained by dynamic rotation of the whole Alq_3 molecule about its *pseudo*-C_3 axis (i.e., *statistically equalizing* the A, B, and C ligands), roughly maintaining its original location. Indeed, crystals of the γ-phase are simply generated by distortion (and slight inflation; see Table 2) of the original triclinic phase, leading to a proper supergroup−subgroup relation to the low-temperature (α) unit cell. Since all diffraction measurements

were performed at ambient temperature, such dynamic disorder is frozen out upon quenching. Therefore, local $\pi-\pi$ contacts occur between statistically occurring A-, B-, and C-type ligands, increasing the flexibility of such links. That the *fac* isomer of Alq_3 is not present in the γ-phase is not obvious from diffraction data; however, we have obtained, upon sublimation at ambient pressure, only powders of (*mer*) α-Alq_3, and this excludes the intermediacy of a different geometric isomer.

Structure of Sublimed Thin Films. Contrary to powders obtained by entrainer sublimation, thin films of Alq_3 (thickness below 100 nm) do not exhibit any X-ray diffraction peaks even for the films deposited at higher substrate temperatures up to 425 K (desorption becomes dominant for T_s above ca. 440 K). Only upon prolongated sublimation (film thickness of several micrometers), some characteristic diffraction peaks of α-Alq_3 are observed. This observation suggests that the α structure is preferentially formed in thin films. At this point, it is worth highlighting the polymorphism of Alq_3 as an intrinsic origin of the amorphous nature of the sublimed thin films. Indeed, as demonstrated above, we found that various molecular packings, involving different quinoxaline pairs of neighboring molecules (A/A′, B/B′, or C/C′), are possible. Moreover, the observation of a partially disordered γ-phase obtained after heating the α-phase above 395 °C demonstrates the possibility of freezing the molecular positions in a disordered manner while cooling the samples. Building up an extended crystalline arrangement of Alq_3 molecules would require a precise ordering of the two enantiomers (present in the starting material) according to one of the possible packings, i.e., a sufficient molecular mobility is required. However, high molecular mobility is strongly hindered by the existence of high energetic barriers due to strong dipole−dipole interactions between Alq_3 molecules (ca. $3-4$ k_BT between two symmetry-related Alq_3 molecules in the α structure). The intrinsic polymorphism and local fluctuations in the enantiomeric concentrations during evaporation, combined with the existence of strong dipolar interactions between Alq_3 molecules,[41] constitute favorable conditions for obtaining glassy amorphous-like films upon sublimation. Accordingly, the assumption of thermal interconversion between *mer*- and *fac*-Alq_3 during sublimation does not appear as a prerequisite for obtaining amorphous thin films.[20]

Summarizing, the different crystal phases of pure or solvated Alq_3 mainly differ in the way asymmetric (±)-*mer-Alq_3 stereoisomers share interatomic contacts with neighboring molecules, i.e., depend on which of the chemically unequivalent A, B, and C rings are used as hinges in building supramolecular entities and further on the whole crystal.*

Spectroscopy. **Optical Absorption and Fluorescence Excitation (FLE) Spectroscopy.** The room-temperature absorption spectra of various Alq_3 systems including solution, thin films, and polycrystalline samples are depicted in Figure 5, the main absorption bands being listed in Table 3. As a general trend, we observe a progressive red shift of the most intense absorption bands when going from the diluted solution to the solid state. The first absorption band shifts from 26 800 cm^{-1} in solution (MeOH, $[Alq_3] = 10^{-4}$ M) to 25 600 cm^{-1} in thin films ($T_s =$ 300 K, thickness of ca. 50 nm) and ca. 24 400 cm^{-1} in the crystalline forms. The most intense absorption band at 39 000 cm^{-1} (Alq_3 in CH_2Cl_2, 10^{-4} M) behaves similarly and is progressively red-shifted to 36 900 cm^{-1} in the crystalline α-Alq_3 while broadening slightly.

In the case of Alq_3 in solution, no obvious band shifts are observed with increasing concentration ($10^{-7}-10^{-2}$ M), but solvents of different polarizabilities and dipolar characters lead to changes of the absorption maxima of up to 1000 cm^{-1}, comparable to those reported for Znq_2.[42] The absorption spectrum of Alq_3 is also found to be quite similar to that of 8-hydroxyquinoline in aqueous solution with pH lower than 6.[43]

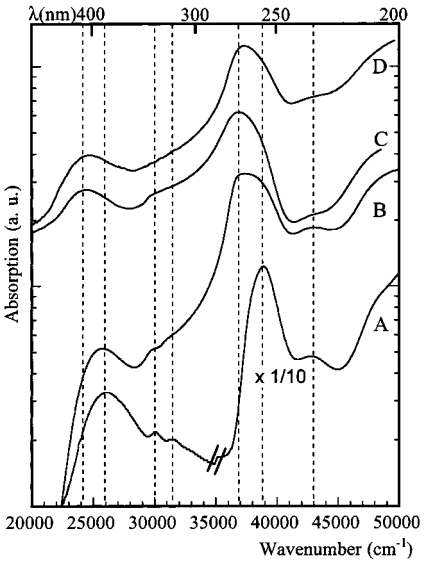

Figure 5. Comparison of the optical absorption spectra of various Alq_3 systems: (A) solution in CH_2Cl_2 (10^{-4} M), (B) thin film on quartz ($T_s = 300$ K, thickness of 50 nm), (C) α-Alq_3, and (D) β-Alq_3. The absorption spectra of α- and β-Alq_3 have been measured on smoothly powdered polycrystalline samples fixed onto a quartz plate.

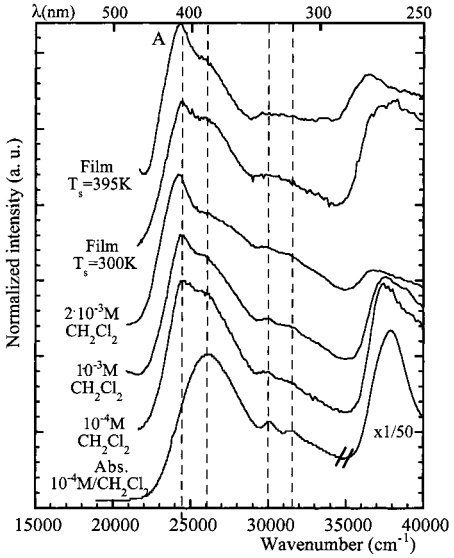

Figure 6. Comparison of the fluorescence excitation (FLE) spectra of Alq_3 in solution at various concentrations and thin films deposited onto passivated Si(100) at $T_s = 300$ K and $T_s = 395$ K and of thickness in the range 50−80 nm. All spectra were obtained at the detection wavelength corresponding to the maximum of fluorescence as listed in Table 4.

As shown in Figure 6, the FLE spectra of the diluted solution (10^{-4} M in CH_2Cl_2) are very similar to the absorption spectrum. The peculiar characteristics of the excitation spectrum are the appearance of a relatively narrow band at 24 400 cm^{-1} (labeled A) corresponding to the onset of absorption, and the decreased intensity of the band at 38 900 cm^{-1}. The additional A band is

(41) Kim, S.-J.; Karis, T. E. *J. Mater. Res.* **1995**, *10*, 2128.

(42) (a) Popovych, O.; Rogers, L. B. *J. Am. Chem. Soc.* **1959**, *81*, 446. (b) McRae, E. G. *J. Phys. Chem.* **1957**, *61*, 562.

(43) Ewing, G. W.; Steck, E. A. *J. Am. Chem. Soc.* **1946**, *68*, 2181.

Table 3. Main Absorption UV−Vis Band Positions for Alq_3 Systems: Solutions, Thin Films and Crystalline Structures (cm^{-1})

system	I (A band)	II	III	IV	V	VI
Solution						
8-hydroxyquinoline in hydrochloric acid (N/100)	24 000	26 500	28 200	40 000		
MeOH (10^{-4} M)	26 800	30 000	31 750	39 200	43 100	48 400
CH_2Cl_2 (10^{-4} M)	26 100	30 050	31 400	38 900	42 750	
Solid State (Amorphous and Polycrystalline)						
thin film/quartz (T_s = 300 K)	25 800	30 050	31 250	37 300	42 900	
α-Alq_3	24 450	29 000		36 900	42 900	
β-Alq_3	24 400	29 000		37 450	43 000	
Alq_3(MeOH)	24 600	29 800		37 300	42 900	
$Alq_3(C_6H_5Cl)_{1/2}$	24 500			37 100	42 300	

Table 4. Positions of the Fluorescence Spectral Maxima for the Various Alq_3 Systems Including Solution in CH_2Cl_2, Thin Films, and the Crystalline Polymorphs (Solvated and Unsolvated) of Alq_3 at 300 and 4.2 K

system	ν_{max}-(300 K)	fwhm-(300 K)	ν_{max}-(4.2 K)	fwhm-(4.2 K)
Solution				
10^{-4} M CH_2Cl_2	19 090	3970	20 700	3870
5×10^{-3} M CH_2Cl_2	18 800	3980		
Thin Film				
T_s=300 K	18 500	4080	19 200	3860
T_s=375 K	19 000	3630	19 380	3470
Crystalline State				
α-Alq_3	19 850	3730	19 850	3510
β-Alq_3	19 400	3760	19 600	3610
Alq_3(MeOH)	19 900	3600	20 250	3560
$Alq_3(C_6H_5Cl)_{1/2}$	20 300	3580	20 250	3530

observed for various solvents regardless of a preliminary degassing of the solution. The FLE spectrum is invariant by scanning the detection wavelength over the whole fluorescence spectrum. We thus infer the existence of a unique electronic origin and accordingly exclude the possibility that the A band originates from chemical impurities. The FLE spectra of the amorphous sublimed thin films are found similar to those of the solutions, reproducing the main features of the absorption spectrum. The reduced intensity of the band located at ca. 37 000 cm^{-1} is most likely a consequence of the high absorption of the UV excitation, i.e., of the limited penetration depth at shorter wavelengths. However, as for the solutions, the A band is present and tends to increase in intensity with increasing substrate temperature T_s. The presence of a similar additional red-shifted band, with respect to absorption, has been reported in the FLE spectrum of polyquinoline[44] as well as in crystalline aromatic rodlike arenedicarboxamides.[11] To highlight the effect of the intermolecular interactions on the optical properties of Alq_3, we have followed the evolution of the FLE spectrum as a function of the concentration of Alq_3 in CH_2Cl_2 solution (in the range 10^{-4} to 2×10^{-3} M). We observe that the A band tends to increase in intensity while shifting slightly to the red with increasing concentration. Whereas the absorption spectra are unaffected by the change of concentration, a red-shift of fluorescence between 19 100 cm^{-1} for $[Alq_3] = 5 \times 10^{-4}$ M and 18 800 cm^{-1} for $[Alq_3] = 5 \times 10^{-3}$ M is observed (see Table 4). The position of the A band in solution and amorphous thin films is found to coincide with the 24 450 cm^{-1} absorption band of the crystalline α-Alq_3. From these observations, we infer that the A band is related to Alq_3 microcrystallites formed upon recrystallization in both solution and amorphous thin films stored in ambient conditions.[45]

Fluorescence. At 300 K. The fluorescence spectra of the unsolvated and solvated crystalline structures, of a sublimed thin film and solution at 300 and 4.2 K, are depicted in Figure 7. The spectroscopic data are collected in Table 4. We first observe that the overall shape of the fluorescence spectra is unaffected by the crystalline packing with a typical full width at half-maximum (fwhm) at 300 K in the range 3580−3780 cm^{-1}. However, the spectral position of fluorescence shows a significant dependence on the crystalline structure. The fluorescence of the denser β-phase is substantially red-shifted (about 450 cm^{-1}) with respect to the α-phase, while both solvated structures show a blue-shifted fluorescence. The different spectral positions of fluorescence observed for the various crystal structures are not attributed to effects of reabsorption since the absorption spectra do not show any significant shifts with crystal structure.

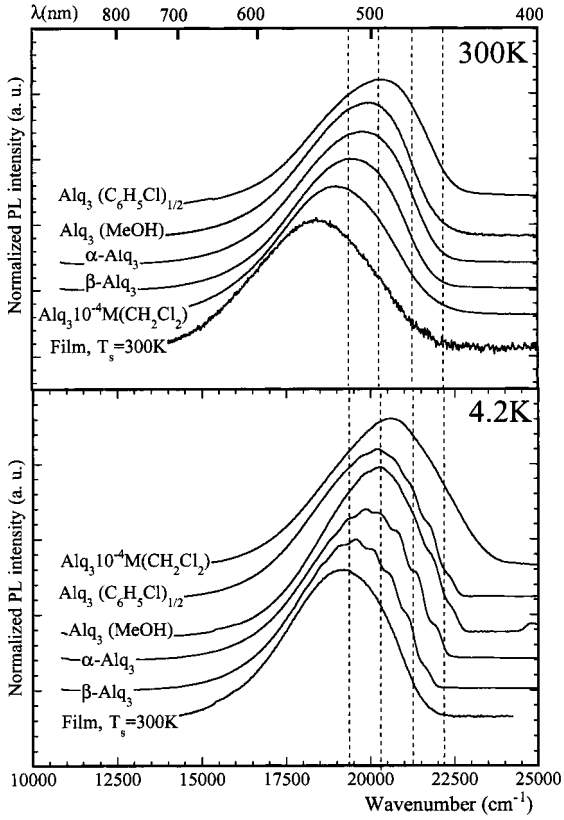

Figure 7. Fluorescence spectra at 300 and 4.2 K for various Alq_3 systems including solution (10^{-4} M in CH_2Cl_2), a thin film onto passivated Si(100) (T_s = 300 K, thickness 50 nm), and different polycrystalline samples of the α- and β-Alq_3 and clathrated Alq_3-$(C_6H_5Cl)_{1/2}$ and Alq_3(MeOH) (excitation energy 27 400 cm^{-1}).

(44) Jenekhe, S. A.; Chen, X. L. *Science* **1998**, *279*, 1903.

(45) (a) Toffolo, F.; Brinkmann, M.; Biscarini, F.; Taliani, C.; Gomes, H.-L.; Aiello, I.; Ghedini, M. *Synth. Met.* **1999**, *101*, 140. (b) Aziz, H.; Popovic, Z.; Hor, A.; Hu, N.-X.; Tripp, C.; Xu, G. *Appl. Phys. Lett.* **1998**, *72*, 756.

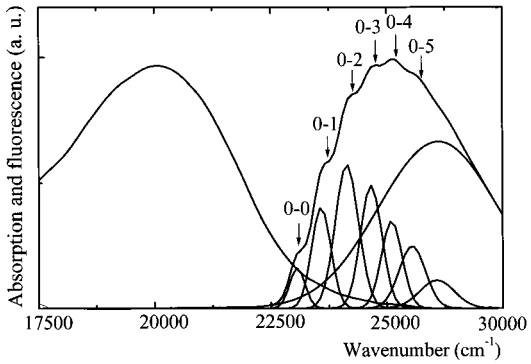

Figure 8. Comparison between the absorption spectrum at 300 K and the fluorescence spectrum at 4.2 K of polycrystalline α-Alq_3. The positions and intensities of the various components of the vibronic structure of fluorescence are collected in Table 5.

Table 5. Spectral Positions and Relative Intensities I_{0n}/I_{00} of the Vibrational Components of the Fluorescence Spectra at 4 K for the α and β Polymorphs of Unsolvated Alq_3[a]

structure	0−0 (cm^{-1})	0−1 (cm^{-1})	0−2 (cm^{-1})	0−3 (cm^{-1})	0−4 (cm^{-1})
α-Alq_3	21 930	21 420	20 890	20 370	19 940
β-Alq_3	21 570	21 150	20 640	20 120	19 690
relative inten I_{0n}/I_{00}	1	2.5	3.7	2.8	

[a] The estimated error on the positions of the vibronic components deduced from the fitting of the fluorescence spectra is ca. 30 cm^{-1}.

The fluorescence of sublimed thin films deposited onto passivated Si(100) (thickness 50−100 nm) has also been investigated. From scanning force microscopy studies,[30] it is found that these films consist of a close packing of amorphous hemispherical droplets characterized by a narrow size distribution and an increasing mean size with substrate temperature T_s (mean radius of ca. 50−100 nm at $T_s = 300$ K and ca. 500 nm at $T_s = 425$ K). We observe that the corresponding fluorescence at room temperature tends clearly to shift to the blue and to narrow slightly upon increasing the substrate temperature from $T_s = 300$ K to $T_s = 375$ K (see Table 4).

At 4.2 K. Lowering the temperature to 4.2 K results in a progressive decrease of the fwhm, which is most pronounced for α-Alq_3, and results in the appearance of a vibronic structure which is identical for single crystals and polycrystalline samples. The vibronic structures of the fluorescence of the unsolvated α and β polymorphs as well as the clathrated forms are similar in both intensity progression and energetical spacings between successive vibronic components (see Figure 8). To analyze this vibronic structure, we have fit the fluorescence spectra of the α and β forms at 4.2 K with 6 Gaussians centered at the most apparent spectral features, and 1−2 additional Gaussian(s) were used for the structureless tail of the spectra. The peak positions obtained from the fitting procedure are listed in Table 5. The relative intensities of the different components should only be considered as rough approximations of the real progression. According to these results, the different vibronic components are found to all be separated from each other by ca. 525 ± 20 cm^{-1} in both the α and β structures. From this result it is inferred that one intramolecular phonon mode is dominantly involved in the observed vibronic structure, independently of the crystal structure. Accordingly, the four main components of this vibronic progression are attributed to the corresponding transitions to the vibronic levels of the ground state, while the higher energy components are assigned to the 0−0 electronic origin of fluorescence in the α and β polymorphs, respectively (see Table 5).

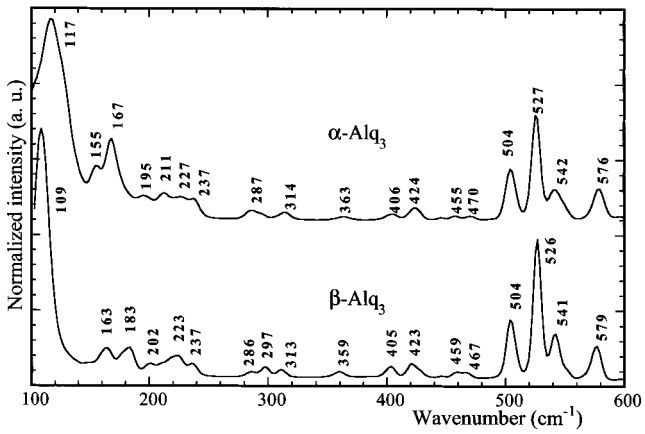

Figure 9. Raman spectra of powdered samples of α and β polymorphs of Alq_3 at 300 K in the 100−600 cm^{-1} range ($\lambda_{exc} = 1064$ nm).

The Raman spectra of the α and β polymorphs of Alq_3, reported in Figure 9, clearly reveal three peaks located at 504, 526, and 541 cm^{-1} for both unsolvated structures. These modes were previously attributed, by comparison with the spectra of naphthalene and quinoxaline, to skeletal in-plane bending of the ligand.[46,48] Preliminary ab initio calculations performed on the hydroxyquinoline ligand and the *mer* isomer of Alq_3 (using the equilibrium molecular geometry obtained from the β structure) confirm the in-plane bending nature of these modes despite the non-strictly-planar geometry of the ligands.[47] Accordingly, since a typical ligand mode is mainly involved in the vibronic structure, we can state the ligand-centered nature of the optically active electronic and vibronic transitions in Alq_3 in agreement with the characteristic fluorogenic character of 8-hydroxyquinoline.[48,49] The contribution of other vibrational modes to the vibronic structure cannot be ruled out. However, the close similarity with the single-mode progression (of about 500 cm^{-1}) observed in the crystalline forms of 9,10-diazaphenanthrene,[13] a heterocyclic and dipolar system, supports our assignment.

From the intensity ratios of the successive components of the vibronic progression relative to the 0−0 transition, we can derive the values of the Franck−Condon factors F_n, which are given by a Poisson distribution ($F_n = e^{-S}S^n/n!$) in the Born−Oppenheimer approximation.[12] The results obtained from various fits show that the F_n progression is well described using a value of the Huang−Rhys factor S of ca. 2.6 ± 0.4, which evidences the strong electron−phonon coupling involving the 525 cm^{-1} bending mode.

As a matter of fact, the vibronic structure is not observed at low temperature neither in liquid solutions (10^{-6}−10^{-4} M in CH_2Cl_2) nor in sublimed thin films (see Figure 7). In solution, this is ascribed to the inhomogeneous broadening resulting from the conformational distribution of Alq_3 molecules, whereas in thin films it reflects the large distribution of molecular environments probed by the Alq_3 molecules.

Raman Spectroscopy (100−300 cm^{-1}). As depicted in Figure 9, the spectra of the Alq_3 polymorphs differ significantly in the 100−300 cm^{-1} range. Marked differences between α and

(46) Rane, A. T.; Ravi, V. V. *Spectrochim. Acta* **1982**, *38*, 937.
(47) Srivastava, S. L.; Prasad, M.; Rohitashava, *Spectrochim. Acta* **1984**, *40*, 681.
(48) Degli Esposti, A.; Brinkmann, M.; Zamboni, R.; Taliani, C.; Muccini, M. *J. Phys. Chem.*, manuscript in preparation.
(49) Bardez, E.; Devol, I.; Larrey, B.; Valeur, B. *J. Phys. Chem. B* **1997**, *101*; 7786.

β polymorphs concern mainly the 109, 117, 156, 167, and 183 cm^{-1} modes. The 117 and 155 cm^{-1} and 109 and 183 cm^{-1} modes can be considered as the characteristic Raman fingerprints of the α and β polymorphs, respectively. As expected, these low-energy modes are highly sensitive to the molecular packing.

Recently ab initio calculations on the *fac* isomer (C_{3v} symmetry) have been performed and the low-energy modes assigned.[50] However, since only the *mer* isomer is evidenced in the various polymorphs of Alq_3, theoretical calculations of the vibrational modes of the *mer* isomer in the different crystal structures are currently in progress and will be reported elsewhere. In particular, we expect significant differences in the degeneracy of the vibrational modes due to the different molecular symmetries of the *mer* and *fac* isomers (C_1 vs C_{3v}), and to the nonplanar geometry of the ligands. We stress that the low-energy modes are very sensitive to the molecular packing, which explains the observed differences in the 100−300 cm^{-1} range of the Raman spectra of the α and β polymorphs.

Discussion

In this section we discuss the effect of the different molecular packings on the optical properties of solid Alq_3, and highlight the intrinsic nature of the solid-state photoexcitations. From Table 1, it stems that the two clathrated forms $Alq_3(C_6H_5Cl)_{1/2}$ and Alq_3(MeOH) show molar volume (V/Z) values of ca. 623 and 593 $Å^3$, i.e., a significantly reduced *molecular* density with respect to the nonsolvated α and β forms characterized by V/Z values of 548 and 536 $Å^3$, respectively. The comparison between the observed values of the density of the different packings (Table 1) and the position of the maximum of the fluorescence reveals a clear correlation: the denser the packing, the more the fluorescence shifts to the red according to the sequence $Alq_3(C_6H_5Cl)_{1/2}$, Alq_3(MeOH), α-Alq_3, and β-Alq_3. A similar effect of the density of the molecular packing on the position of the fluorescence maximum has been reported in various crystalline forms of *trans*-stilbene derivatives with typical shifts of up to 2000 cm^{-1}.[11]

A closer insight into the various crystalline structures reveals the existence of close contacts between pairs of quinoxaline ligands Q/Q′ belonging to neighboring Alq_3 molecules with interligand spacings in the range 3.9−3.5 Å. By comparison between the fluorescence and the geometrical characteristics of the Q/Q′ moieties, we find that the β structure where the $\pi-\pi$ overlaps are most favorable (two quinoxaline ligands per Alq_3 molecule are involved in 3.5 Å contacts) is also the one showing the most red-shifted fluorescence. However, contrary to stilbene derivatives where a clear dimer emission band is observed in fluorescence,[11] no such dimer emission is observed in any of the crystalline forms of Alq_3. In fact, the fluorescence emission is nearly a mirror image of absorption, and it shows a clear vibronic structure at low temperature. These fluorescence characteristics, together with the in-plane nature of the dominant vibrational mode involved in the vibronic coupling, rule out any significant dimer emission. Moreover, solid-state excimer emission can also be discarded by several experimental facts. Excimer states are dissociative in their ground state and their strongly red-shifted emission is structureless, in clear disagreement with our observations.

In the clathrated forms, most of the ligands are involved in Q/S/Q′ sequences, and pairs of quinoxaline dimers with short contacts of ca. 3.6 Å are only observed along the (100) direction. In the case of Alq_3(MeOH), the methanol molecules cannot lead to any $\pi-\pi$ orbital overlaps with the ligands and simply act as spacer molecules, reducing the direct intermolecular interactions between quinoxaline moieties. In the case of $Alq_3(C_6H_5Cl)_{1/2}$, however, specific S/Q overlaps with a distance of ca. 3.6 Å are involved in the Q/S/Q′ sequences. Nevertheless, the large energy difference between the electronic states of Alq_3 and C_6H_5Cl (first absorption band at ca. 37 000 cm^{-1}) implies that the guest C_6H_5-Cl molecules act as spacer molecules, in the same way as MeOH. Accordingly, it comes out that the emission of solid Alq_3 can be blue-shifted by introducing optically inactive spacer molecules in the crystalline network. A similar effect can be expected in thin films if such spacer molecules are introduced by coevaporation.

The optical properties in thin films are strictly related to their amorphous nature. Unlike the crystal structures in which the relative orientations of molecules are strictly defined, a large distribution of molecular packings is possible in the amorphous films. Within the broad distribution of molecular packings, favorable $\pi-\pi$ overlaps between facing ligands may occur, which are responsible for the strongly red shifted fluorescence observed for the films obtained at $T_s = 300$ K. Moreover, the large distribution of molecular environments results in the broadening of the fluorescence spectra, and in the smearing out of any vibronic structure. As T_s is increased, the molecular mobility promotes a preferential rearrangement of the molecules toward the α crystalline form, which is obtained upon prolonged sublimation (vide supra). We accordingly ascribe the observed blue shift and narrowing of the thin film fluorescence with increasing T_s to a more defined molecular packing and environment. A similar scenario may be proposed to explain the origin of the blue shift of fluorescence (ca. 300−800 cm^{-1}) observed in multiple quantum wells involving Alq_3 layers of decreasing thickness.[51]

Conclusions

Three novel crystal structures of unsolvated Alq_3 have been synthesized, and their crystal structure has been refined from powders and single-crystals, evidencing the intrinsic polymorphism of Alq_3. These structures consist of a racemic mixture of *mer*-Alq_3 and are characterized by different molecular densities and $\pi-\pi$ short contacts between adjacent quinoxaline ligands. The structural results of this study highlight the power of the newly emerging ab initio X-ray powder diffraction technique on conventional laboratory equipment.[52] Obviously, the major output of XRPD studies frequently cannot lie in the precise description of the *intra*molecular geometry since heavy idealization of the structural fragments is often necessary.[53]

(50) Halls, M. D.; Aroca, R. *Can. J. Chem.* **1998**, *76*, 1730.

(51) Hy, A.; Chen, B. J.; Hou, J. Y.; Liu, S. Y. *J. Phys. D*: *Appl. Phys.* **1998**, *31*, 1144. (b) Mori, T.; Obata, K.; Miyachi, K.; Mizutani, T.; Kawakami, Y. *Jpn. J. Phys*. **1997**, *36*, 7239.

(52) The fortunate occurrence of single crystals of the β-phase and of a number of solvated Alq_3 forms allowed the easy formulation of its *molecular* geometry, which has been successfully used in modeling the rather complex diffraction pattern of α-Alq_3 (34 crystallographically independent non-hydrogen atoms). The very same approach led recently to the structural characterization of $[Pd(Hdmpz)_2(dmpz)_2]_2$ (γ-phase, 58 non-H atoms; Masciocchi, N.; Ardizzoia, G. A.; La Monica, G.; Moret, M.; Sironi, A. *Inorg. Chem*. **1997**, *36*, 449) and of fluticasone propionate, a complex steroid (34 non-H atoms; Kariuki, B.; Psallidas, K.; Harris, K. D. M.; Johnston, R. L.; Lancaster, R. W.; Staniforth, S. E.; Cooper, S. M. *Chem. Commun*. **1999**, 1677).

(53) See, for example, the chemically implausible C−C distances (1.62−1.68 Å) recently proposed from very good quality synchrotron data of lithium halogenoacetates with only six independently refined atoms (Ehrenberg, H.; Hasse, B.; Schwarz, K.; Epple, M. *Acta Crystallogr*. **1999**, *B55*, 517).

(54) Wang, Y.; Zhang, W.; Li, Y.; Ye, L.; Yang, G. *Chem. Mater*. **1999**, *11*, 530.

However, relevant packing features, such as those discussed in this paper are satisfactorily refined from X-ray powder diffraction data.

Given the different solvated and unsolvated molecular structures, we have analyzed the effect of molecular packing on the optical properties by using absorption, fluorescence excitation, fluorescence, and Raman spectroscopies. Despite the existence of short contacts between quinoxaline ligands of adjacent Alq_3 molecules (3.5−3.9 Å), neither excimer nor typical dimer emissions are observed in the crystalline phases of Alq_3. The vibronic structure of the fluorescence is observed for the first time at low temperature (4.2 K) in the solvated and unsolvated polymorphs of Alq_3. It supports the ligand-centered nature of the optically active electronic transitions in Alq_3 and is analyzed in terms of a Franck−Condon coupling involving a skeletal in-plane bending mode of the ligand at ca. 525 cm^{-1}. A Huang−Rhys factor of ca. 2.6 is derived from the Franck−Condon factor progression, highlighting the strong electron−phonon coupling of the active vibronic transition. A clear identification of the α and β polymorphs is derived from the analysis of the low-energy range (100−300 cm^{-1}) of the Raman spectra. The amorphous nature of the sublimed thin films is explained in terms of (i) the intrinsic polymorphism of Alq_3, (ii) the racemic nature of the source material used for sublimation, and (iii) the strong dipolar interactions between Alq_3 molecules.

Acknowledgment. We acknowledge support by the European Union-Training and Mobility for Researchers program on Synthetic Electroactive Organic Architectures (SELOA) FRX-C.T.900096 and PF MSTA II progetto coordinato DEMO. Fruitful discussion with R. Zamboni and the technical support of Mr. G. Mezza are also gratefully acknowledged.

Supporting Information Available: Lists of fractional atomic coordinates for Alq_3 (α-, and β-phases C_6H_5Cl-clathrated phases) (PDF) and full list of bond lengths and angles for β-Alq_3 (CIF). This material is available free of charge via the Internet at http://pubs.acs.org.

JA993608K